MRI – Review´s manuscript

Estefanía Alejandra Hernández-Rangel[1], José Emmanuel Chávez-Zepeda[1], Rafael Guzman-Cabrera[2], Blanca Olivia Murillo-Ortiz[3], Huetzin Aaron Prez-Olivas[1], and Teodoro Córdova-Fraga[1*]

[1]Departamento de Ingeniería Física, Universidad de Guanajuato campus León, Loma del Bosque 103, Lomas del Campestre, 37150 León, GTO, Mexico.

[2]División de Ingenierías, Universidad de Guanajuato campus Irapuato-Salamanca, Carretera Salamanca-Valle de Santiago, km. 3.5 + 1.8. Comunidad de Palo Blanco, 36885 Salamanca, GTO, México.

[3]Unidad de Investigación Médica, UMAE No. 1 Bajío, OOAD Guanajuato. Av. Insurgentes y Blvd. López Mateos s/n, Los Paraísos 37328 León GTO, México.

[*]Corresponding author: Teodoro Córdova-Fraga

Abstract Magnetic Resonance Imaging (MRI) is a non-invasive modality whose signal formation emerges from the quantum mechanical properties of nuclear spin and its interaction with static and time-varying magnetic fields. This review synthesizes core principles—from nuclear spin, Zeeman energy splitting, and Larmor precession to radiofrequency (RF) excitation, relaxation processes (T_1, T_2, T_2^*), spatial encoding with gradients, and the principal contrast mechanisms used in clinical practice. We complement this conceptual framework with illustrative calculations at 3 T, including the Zeeman energy difference and the resulting Boltzmann population imbalance, to demonstrate how a minute statistical excess of aligned spins (on the order of ~10 per million) nevertheless produces a measurable and clinically useful MR signal. We then connect these foundations to image formation and diagnostic contrast, linking physics concepts to representative clinical applications across neurology, musculoskeletal imaging, cardiovascular MRI, spectroscopy, and interventional MRI. Finally, we discuss practical trade-offs associated with increasing field strength (*e.g.*, SNR, SAR, susceptibility, B_0/B_1 inhomogeneity) and outline opportunities in quantitative and advanced reconstruction methods. Overall, this work provides a concise, integrated account of MRI physics that bridges fundamental spin dynamics with image contrast and clinical utility.

Keywords: nuclear spin; Zeeman splitting; Larmor precession; relaxation (T_1, T_2, T_2^*); gradient encoding; gyromagnetic ratio.

Introduction

Medical imaging provides a unique, non-invasive window into the human body, enabling clinicians and researchers to diagnose, monitor, and study disease with increasing precision. Among the various modalities available, Magnetic Resonance Imaging (MRI) has emerged as one of the most versatile and powerful tools in contemporary clinical practice (Katti *et al*., 2011). Its operation is grounded in quantum mechanical principles, specifically the intrinsic spin of hydrogen nuclei abundant in water and fat molecules. When these nuclei are subjected to a strong external magnetic field—typically on the order of several Teslas—and stimulated with radiofrequency pulses, they emit detectable signals that reflect their local molecular environment.

Through sophisticated signal-processing and reconstruction techniques, these signals are transformed into images that exquisitely depict the spatial distribution of water within tissues (Liang & Lauterbur, 2000). MRI offers remarkable flexibility in selecting imaging planes and contrast mechanisms, and unlike computed tomography, it achieves this without exposing patients to ionizing radiation (Cherry *et al*., 2012). Its superior soft-tissue contrast enables fine differentiation among normal and

pathological tissues, making MRI indispensable in fields such as neurology, oncology, cardiology, and musculoskeletal imaging (Edelman & Warach, 1993).

Beyond its clinical utility, MRI represents a landmark in the convergence of nuclear physics, engineering, mathematics, and medicine. Continuous advances in magnet technology, pulse sequence design, and computational reconstruction further expand their capabilities, ensuring that MRI remains a cornerstone of modern biomedical imaging.

Background

The physical foundations of MRI lie at the intersection of classical electromagnetism and quantum mechanics. The underlying phenomenon, originally known as Nuclear Magnetic Resonance (NMR), was first demonstrated in liquids in 1946 (Weingärtner, 2013). This landmark discovery is attributed to Felix Bloch, who detected the characteristic NMR signal using an apparatus of his own design—famously observing the effect when he placed his water-rich fingertip inside the device (Rabi, 2025).

A major conceptual leap occurred in 1973, when Paul Lauterbur introduced the use of gradient magnetic fields to spatially encode NMR signals. This innovation enabled the reconstruction of the first NMR image, establishing the essential framework for modern MRI technology (Dawson, 2013). Lauterbur's insights provided the missing link between the physics of nuclear magnetism and practical imaging of biological tissues.

During the 1980s, the technique underwent a strategic rebranding. The term Magnetic Resonance Imaging (MRI) replaced "Nuclear Magnetic Resonance Imaging" to avoid negative public reactions tied to the word nuclear, which was commonly (but incorrectly) associated with harmful ionizing radiation. MRI relies on non-ionizing radiofrequency fields and is considered medically safe (Rinck, 2018). This change in terminology was essential for differentiating MRI from nuclear medicine procedures and ensuring widespread clinical acceptance.

Today, MRI stands not only as a product of decades of scientific innovation but also as a testament to the synergy between physics, engineering, and biomedical research. Its development—from Bloch's foundational experiments to Lauterbur's imaging breakthrough—has transformed NMR from a laboratory curiosity into one of the most sophisticated diagnostic tools in modern medicine.

Nuclear Spin

Nuclear spin is a fundamental quantum-mechanical property of atomic nuclei and has no classical analog, although it is often compared conceptually to angular momentum. For protons and neutrons, this intrinsic spin is a quantized parameter. In particular, the hydrogen nucleus—a single proton of central relevance to medical imaging—has a spin quantum number $S = ½$, which yields two allowable spin states: $+½$ and $-½$ (Hughes *et al*., 2009).

A crucial consequence of this intrinsic spin is the presence of a magnetic dipole moment (μ). Because the proton carries an electric charge and spins about its axis, it behaves like an extremely small magnetic bar magnet, generating a magnetic moment aligned with its spin direction (Bibiloni *et al.*, 2003). This dipole moment forms the physical basis of nuclear

magnetic resonance, as it enables nuclei to interact with external magnetic fields in quantifiable and detectable ways.

In the context of medical imaging, the hydrogen proton is the nucleus of greatest importance for MRI. This is due to its large magnetic moment, its high sensitivity to NMR excitation, and its remarkable natural abundance throughout the human body, predominantly in water and lipid molecules (Haacke *et al.*, 1999). When placed in a strong magnetic field, the enormous ensemble of hydrogen nuclei—each acting as a microscopic magnetic dipole—collectively contributes to the macroscopic magnetization from which MRI signals originate.

Thus, the basic MRI signal arises from the coordinated behavior of billions of nuclear spins, whose interactions with magnetic fields and radiofrequency energy enable the generation of detailed anatomical and physiological images.

Static Field and Larmor Precession

A strong and homogeneous static magnetic field ($\vec{B}_0$) is the fundamental requirement for NMR and, by extension, for MRI. In clinical systems, the field strength is a critical determinant of image quality because it directly influences the signal-to-noise ratio (SNR). Modern diagnostic scanners typically operate between 0.5 T and 3.0 T, with 1.5 T scanners serving as the standard for general clinical practice. Systems operating at 3.0 T provide increased SNR and improved spatial resolution, making them particularly valuable in applications such as neuroimaging, small-structure musculoskeletal studies, and advanced functional imaging (Brown *et al*., 2014).

When nuclei with non-zero spin—most notably the abundant hydrogen-1 proton—are placed within the static magnetic field, they behave as microscopic magnetic dipoles. Quantum mechanics dictates that these dipoles can occupy only two discrete spin energy states: one aligned with $\vec{B}_0$ (the lower-energy state) and the other anti-aligned (the higher-energy state). The emergence of these two energy levels is a direct manifestation of the Zeeman effect, which describes the splitting of magnetic energy states in the presence of an external magnetic field (Crutcher *et al*., 2019). Importantly, the energy difference (ΔE) between these states is linearly proportional to the magnitude of $\vec{B}_0$, implying that higher field strengths produce greater population differences and consequently stronger measurable magnetization.

$$\Delta E = \hbar\omega_0$$

This quantum description is intimately linked to the classical picture of Larmor precession. Instead of remaining static, the magnetic moments of the nuclei precess around the direction of the external field much like a spinning top precesses under the influence of gravity. This motion occurs at a precise angular frequency known as the Larmor frequency (ω_0), defined by the fundamental relation:

$$\omega_0 = \gamma B_0$$

where γ is the gyromagnetic ratio, a nuclear property that determines how strongly a nucleus interacts with a magnetic field. The Larmor frequency represents the resonant frequency at which MRI systems apply radiofrequency (RF) pulses to perturb the nuclear spins. When the RF pulse matches ω_0, it induces transitions between the Zeeman energy states, thereby generating the coherent nuclear magnetization that produces the detectable MRI signal.

Thus, the interplay between the static field, energy level splitting, and Larmor precession forms the physical basis for spin excitation, signal formation, and ultimately the image contrast mechanisms leveraged in MRI

The interaction between the static magnetic field ($\vec{B}_0$) and the nuclear magnetic moment produces a torque that prevents the moment from simply aligning with the field. Instead, the magnetic moment undergoes a steady rotational motion known as precession, tracing a conical path around the direction of the applied field in a manner analogous to a gyroscope under gravity (Edmonds, 1993). Because the Larmor frequency is directly proportional to $\vec{B}_0$, higher field strengths yield proportionally higher precessional frequencies. For example, hydrogen protons precess at approximately 63.9 MHz in a 1.5 T magnetic field and at roughly 127.7 MHz in a 3.0 T system (Hoult & Bhakar, 1997). These frequencies determine the energy required for resonance and influence the achievable signal-to-noise ratio, thereby impacting overall imaging performance.

In figure 1 a schematic representation of the Larmor precession motion is shown, where it can be seen how the nuclear magnetic moment describes a conical motion around the static field $\vec{B}_0$, illustrating the rotating nature and characteristic frequency of this fundamental dynamic in magnetic resonance.

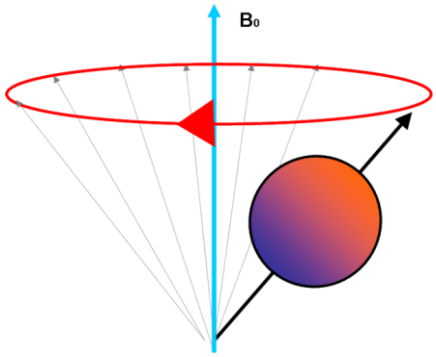

Figure 1. The Precession of Larmor representation.

Due to the energy difference (ΔE) between the spin states in a magnetic field, the nuclear spins do not align uniformly with the external field (see Figure 2). Instead, a slightly greater number of nuclei occupy the lower-energy state, aligning parallel to the static magnetic field $\vec{B}_0$, while fewer occupy the higher-energy anti-parallel state. This produces a small but significant population imbalance. Figure 2 shows that the net magnetization will be 0, since all pairs of magnetizations cancel each other out.

Although individual nuclear magnetic moments precess randomly about the axis of $\vec{B}_0$, their transverse components cancel one another out. The opposing spin orientations balance in pairs; however, the slight excess of spins aligned with the field yields a non-zero resultant vector. This ensemble effect gives rise to the Net Magnetization (NM), which points along the $+z$ axis, parallel to the direction of the main magnetic field.

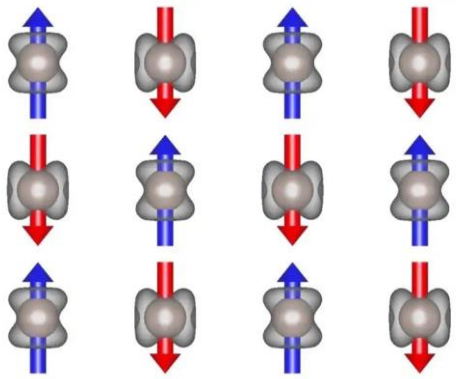

Figure 2. Origin of net magnetization (NM).

This net magnetization forms the primary source of the measurable MRI signal, even though the surplus represents only a few additional aligned spins per million. It is this minuscule collective imbalance—amplified by the immense number of nuclei in biological tissue—that makes magnetic resonance detectable and enables the rich contrast mechanisms used in Magnetic Resonance Imaging.

Radiofrequency Field

As already stated, the fundamental phenomenon of resonance in NMR and its application in MRI occurs when an externally applied radiofrequency (RF) pulse matches the precise Larmor frequency (ω_0) of the specific nuclei being studied (Rigden, 1986). The Larmor frequency is intrinsically dependent on the strength of the main static magnetic field ($\vec{B}_0$) and the gyromagnetic ratio of the nucleus, a unique constant for each atomic type. This RF pulse is not a simple, continuous wave but a carefully calibrated electromagnetic burst transmitted through a dedicated coil or antenna, often designed as a resonator to maximize efficiency.

When the RF pulse is applied at the resonant Larmor frequency, it delivers the exact quantum of energy required to promote nuclei from the lower-energy, parallel spin state to the higher-energy, anti-parallel state. This absorption of energy does not occur for individual spins in isolation but has a direct, coherent effect on the macroscopic net magnetization vector (M). The primary action of the RF pulse is to "tip" this net magnetization away from its equilibrium position along the positive $z-$axis (aligned with B_0). As the net magnetization vector is deflected, it begins to precess around the $z-$axis, tracing a conical path and generating a component in the transverse plane ($xy-$plane). This newly created component is known as the transverse magnetization (M_{xy}), as illustrated in Figure 3.

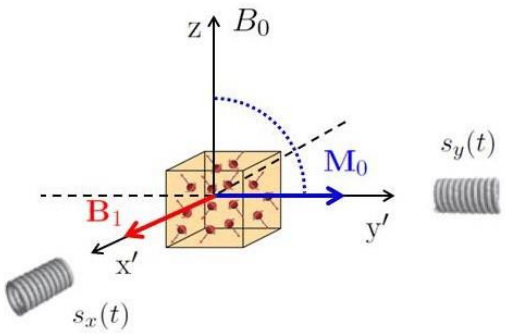

Figure 3. Representation of the transverse magnetization of the proton.

The precession of this transverse magnetization is crucial, as a moving magnetic field induces an electrical current in a receiver coil—the fundamental signal detected in MRI. The magnitude of the transverse magnetization is directly determined by the amplitude and duration of the RF pulse; a 90 −degree pulse, for instance, tips the entire net magnetization completely into the transverse plane, maximizing the detectable signal. This excitation process is the essential first step that allows for spatial encoding and image formation in clinical and research MRI.
Furthermore, the transverse component of magnetization, M_{xy}, is the one responsible for generating the detectable NMR signal through electromagnetic induction (Cobas, 2020).

Relaxation Times

Once the radiofrequency pulse is removed, the nuclear spins gradually return to their thermal equilibrium state (Vasanawala, Pauly, & Nishimura, 1999). This recovery occurs through two fundamental and simultaneous relaxation processes: T_1 (spin–lattice relaxation) and T_2 (spin–spin relaxation). These mechanisms describe how the longitudinal and transverse components of magnetization evolve over time and are essential for understanding image contrast in MRI.

- **T_1 Relaxation** (*Spin–Lattice Relaxation*)
  T_1 relaxation describes the recovery of longitudinal magnetization (M_z) as the excited spins release energy to their surrounding molecular environment, known as the lattice. This process governs how quickly the net magnetization realigns with the static magnetic field $\vec{B}_0$. T_1 is defined as the time required for M_z to recover to approximately 63 % of its equilibrium value. The rate of T_1 relaxation depends heavily on tissue composition, molecular tumbling rates, and magnetic field strength (Bloembergen, Purcell, & Pound, 1948; Haacke et al., 1999).
- **T_2 Relaxation** (*Spin–Spin Relaxation*)
  T_2 relaxation refers to the decay of transverse magnetization (M_{xy}) caused by the progressive dephasing of individual nuclear magnetic moments. Unlike T_1, this process does not involve energy transfer to the lattice; instead, it arises from spin–spin interactions that produce local magnetic field inhomogeneities. T_2 is defined as the time required for M_{xy} to decrease to approximately 37 % of its initial value (Haacke *et al.*, 1999; Edelman & Warach, 1993). Because dephasing typically occurs more rapidly than longitudinal recovery, T_2 values are always less than or equal to T_1 values.

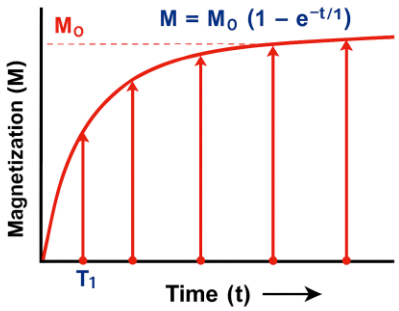

Figure 4. Graph of T_1 (Spin–Lattice) Relaxation.

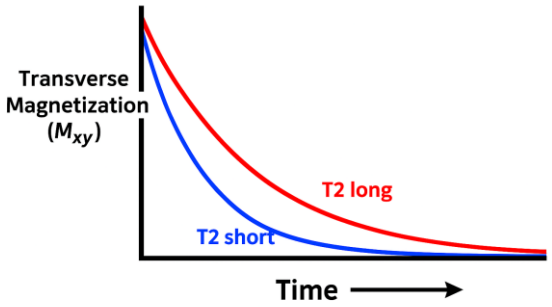

Figure 5. Graph of T_2 (Spin–Spin) Relaxation.

These two relaxation mechanisms form the physical basis for numerous MRI contrast strategies, as tissues with distinct T_1 and T_2 properties exhibit markedly different signal intensities across pulse sequences. In general, relaxation behavior depends strongly on the physicochemical environment of the nucleus and the specific tissue being analyzed, making T_1 and T_2 the primary sources of contrast in MRI. This leads to a well-established general trend

$$T_1 \gg T_2$$

Image Formation in MRI

In Magnetic Resonance Imaging, the raw Nuclear Magnetic Resonance signal contains no inherent spatial information. Without additional encoding steps, it would be impossible to assign signal intensity to specific locations within the body. Spatial information is introduced through the use of magnetic field gradients, which are weak, temporary magnetic fields that vary linearly across the imaging volume. When gradients are applied at different stages of the imaging process, the Larmor frequency becomes position-dependent, allowing spatial localization of the MR signal (Gudiño *et al*., 2023).

Larmor Frequency Under a Gradient Field

When a magnetic field gradient G_x is applied along the x −direction, the local magnetic field becomes:

$$B(x) = B_0 + G_x x$$

Thus, from the Larmor equation, the position-dependent precessional frequency is:

$$\omega(x) = \gamma\, B(x) = \gamma(\, B_0 \, + \, G_x \, x \,)$$

This linear relationship between frequency and spatial position forms the basis for MRI spatial encoding.

Purposes of Gradient Fields

Magnetic field gradients are applied during specific parts of the pulse sequence to control where spins are excited, how signal is spatially encoded, and how it can be reconstructed. Their major functions are described below.

1: *Slice Selection*

Slice selection is achieved by applying a gradient (commonly along the $z-$ axis, G_z) simultaneously with a frequency-selective *RF* pulse. Because the gradient causes the local Larmor frequency to vary with position, only spins whose frequencies fall within the *RF* pulse bandwidth are exciting. The excited slice has a thickness:

$$\Delta z = \frac{\Delta f}{\gamma G_z}$$

where Δf is the pulse bandwidth, and G_z is the slice-selection gradient amplitude

This process allows selective excitation of thin anatomical slices (Haacke *et al*., 1999; Bernstein, King, & Zhou, 2004).

2. *Frequency Encoding* (*Readout Gradient*)

During the acquisition of the *MR* signal, a gradient (typically G_x) is applied so that spins at different x positions precess at different frequencies. The measured signal is a superposition of these frequencies:

$$s(t) = \int \rho(x) e^{i\gamma G_x x t}\, dx$$

is applying a Fourier Transform to the acquired signal decomposes it into its spatial frequency components, enabling reconstruction of spatial distribution along the readout direction (Gallagher *et al*., 2008).

Phase Encoding

Phase encoding is achieved by applying a gradient (commonly G_y) briefly before signal readout. During its duration Δt, spins accumulate a spatially dependent phase shift:

$$\phi(y) = \gamma G_y y \Delta t$$

By repeating the acquisition with multiple values of G_y, different phase shifts are encoded across the tissue. These distinct phase steps allow reconstruction of the second spatial dimension in k-space (Bernstein *et al*., 2004; Liang & Lauterbur, 2000).

Image Contrast Parameters in MRI

MRI image contrast arises primarily from deliberate manipulation of the fundamental relaxation properties of tissues. The most influential parameters governing contrast are the longitudinal relaxation time (T_1), the transverse relaxation time (T_2), and the spin–spin decay time (T_2^*), as well as proton density and specific pulse-sequence design choices. By adjusting imaging parameters such as the repetition time (TR), echo time (TE), and flip angle, different tissues can be made to appear brighter or darker depending on their intrinsic relaxation characteristics (Bernstein, King, & Zhou, 2004; Haacke *et al.*, 1999).

T_1 −weighted contrast enhances differences in the rate at which tissues recover longitudinal magnetization. Tissues with short T_1 values (*e.g.*, fat) recover quickly and appear bright, whereas those with long T_1 values (*e.g*., CSF) appear dark.

T_2 −weighted contrast reflects differences in the decay of transverse magnetization. Fluids, which have long T_2 times, appear bright, while tissues with shorter T_2 values exhibit lower signal intensity.

T_2^* −weighted contrast is sensitive to local magnetic field inhomogeneities and susceptibility effects, making it useful for detecting hemorrhage, calcifications, or changes in deoxyhemoglobin concentration (Ogawa *et al*., 1990).

Additionally, contrast can be modulated through proton density weighting, inversion recovery sequences, and the administration of paramagnetic contrast agents such as gadolinium-based compounds. These agents shorten $T1$ relaxation, thereby increasing signal intensity in areas where they accumulate (Runge, 2018). Understanding how pulse sequence parameters interact with tissue properties enables precise tailoring of contrast to specific diagnostic goals.

Clinical Applications of MRI

MRI is widely employed across numerous medical specialties due to its excellent soft-tissue contrast, lack of ionizing radiation, and versatility in exploiting different physical mechanisms to generate contrast. Key clinical applications include:

Neurology: MRI is the modality of choice for imaging the central nervous system. It is indispensable in evaluating brain tumors, multiple sclerosis, stroke, and structural malformations. Advanced techniques such as diffusion-weighted imaging (DWI) and

susceptibility-weighted imaging (SWI) enhance the detection of ischemic injury and microhemorrhages (Barkhof *et al*., 2012; Filippi *et al*., 2019).

Orthopedics and Musculoskeletal Imaging: MRI provides excellent visualization of the muscles, tendons, ligaments, cartilage, and bone marrow, making it essential for diagnosing ligament tears, meniscal injuries, rotator cuff pathology, and stress fractures. Its multiplanar capability allows comprehensive evaluation without ionizing radiation (Kijowski *et al*., 2014).

Cardiovascular MRI (CMR): Cardiac MRI enables noninvasive assessment of cardiac morphology, myocardial viability, perfusion, congenital abnormalities, and coronary artery disease. MR angiography (MRA) provides high-resolution images of blood vessels without the risks associated with iodinated contrast media (Puntmann *et al*., 2020).

Functional MRI (fMRI): Functional MRI measures brain activity by detecting blood oxygenation level–dependent (BOLD) contrast, which reflects changes in deoxyhemoglobin concentration. fMRI is widely used in cognitive neuroscience, pre-surgical planning, and the study of sensory, motor, and language networks (Logothetis, 2008).

Magnetic Resonance Spectroscopy (MRS): MRS allows non-invasive biochemical analysis of tissues by detecting small frequency shifts related to different molecular environments. It provides insight into metabolite concentrations, enabling evaluation of tumors, epilepsy, metabolic disorders, and ischemia (Danielsen & Ross, 1999).

Interventional MRI (iMRI): Technological advances, including open magnet designs and MRI-compatible surgical tools, allow real-time MRI guidance for biopsies, tumor resections, minimally invasive procedures, and even some open surgical interventions. iMRI improves precision and outcomes by providing continuous high-contrast imaging (Jolesz, 2011)

MRI Calculations

Estimation of Energy States and Proton Angular Orientation

For a hydrogen nucleus (^1H), which contains a single proton, the following physical constants and approximations are considered:

Gyromagnetic ratio:

$$\gamma \approx 2.675 \times 10^8 \text{ rad}\cdot\text{T}^{-1}\text{s}^{-1}$$

k_B Boltzmann constant:

$$k_B \approx 1.3806 \times 10^{-23} \text{ J}\cdot\text{K}^{-1}$$

Reduced Planck constant:

$$\hbar \approx 1.0548 \times 10^{-34}\ \text{J·s}$$

Physiological temperature:

$$T \approx 310\ \text{K}$$

Static magnetic field:

$$B_0 \approx 3\ \text{T}$$

The precession angle θ is determined from the ratio of the magnetic quantum number to the spin quantum number. This angular parameter depends solely on the spin system and is independent of the magnitude of the external field $\vec{B}_0$:

$$\cos\theta = \frac{m_I}{\sqrt{I(I+1)}} = \pm\frac{1}{3}$$

This expression yields two allowable orientations for the proton magnetic moment:

- $\theta \approx 54.74^\circ$— corresponding to the lower-energy (aligned) state
- $\theta \approx 156.26^\circ$— corresponding to the higher-energy (anti-aligned) state

These angles reflect the quantized nature of the spin-½ system.

Energy Difference Between Spin States

The energy separation between the aligned and anti-aligned spin states can be obtained using the Zeeman relation:

$$\Delta E = \hbar\gamma B_0$$

Substituting the physical constants:

$$\begin{aligned}\Delta E &= (1.0549 \times 10^{-34}\ \text{J·s})\left(2.675 \times 10^{8}\ \text{rad·T}^{-1}\text{s}^{-1}\right)(3\ \text{T}) \\ &\approx 8.46 \times 10^{-26}\ \text{J}\end{aligned}$$

This extremely small energy gap underlies the low population difference between spin states at thermal equilibrium—an essential consideration in magnetic resonance signal generation.

Contributing Protons to Magnetization (3 T)

The net magnetization NM arises from the slight population imbalance between the two spin states, as described by the Boltzmann distribution.

The relative excess of spins in the lower-energy state is given by:

$$\frac{N_\uparrow - N_\downarrow}{N_s} \approx \frac{\Delta E}{2k_B T} = \frac{\hbar\gamma B_0}{2k_B T}.$$

Using the previously defined constants and substituting the numerical values—expressing the result as a fraction per million spins—it is obtained:

$$\frac{N_{\uparrow} - N_{\downarrow}}{N_s} = \frac{8.46 \times 10^{-26}\text{J}}{2(1.3806 \times 10^{-23}\,\text{J} \cdot \text{K}^{-1})(310\,K)} = 9.89 \approx 10 \text{ protons per million}$$

This result highlights the extremely small population difference responsible for generating measurable net magnetization in MRI, even under a strong static magnetic field of 3T.

Contextualization of Proton Contributions to Net Magnetization

To better illustrate the practical implications of the calculated population difference between spin states, it is useful to relate these results to realistic anatomical dimensions. Consider the following representative parameters commonly assumed in MRI modeling:

- An adult individual with a body mass of approximately 70 kg.
- A human brain weighing roughly 1.5 kg, consistent with standard neuroanatomical estimates.
- A slice thickness of 1 mm, corresponding to the resolution typically associated with a single voxel in high-resolution MRI acquisitions.

Although a voxel contains only a minute fraction of the brain's total tissue mass, the number of hydrogen nuclei within such a small volume is still extraordinarily large due to the high-water content and dense molecular structure of biological tissues. When the Boltzmann distribution predicts an excess of approximately 10 lower-energy protons per million, this difference may appear negligible from a microscopic perspective. However, within the macroscopic context of MRI, this minute population imbalance becomes highly significant.

Even in a $1-\text{mm}-$thick voxel, the total number of protons is on the order of 10^{20} to 10^{21}, meaning that the slight statistical excess translates into trillions of contributing spins. This collective imbalance is what ultimately generates a nonzero net magnetization vector, which then precesses around the static magnetic field $\vec{B}_0$. The combined effect of these spins produces an electromagnetically measurable signal, which is subsequently amplified, filtered, and reconstructed into high-quality MR images.

Thus, despite the extremely small energy difference between the spin states and the correspondingly small fractional population excess, the sheer magnitude of contributing protons ensures that the MRI system can acquire a robust and detectable signal. These considerations emphasize the remarkable sensitivity of magnetic resonance techniques: a phenomenon rooted not in the magnitude of microscopic interactions but rather in the overwhelming abundance of participating nuclear spins.

Discussion

Physical implications of spin population imbalance

The numerical example at 3 T underscores a central MRI paradox: although the Zeeman energy gap is exceedingly small and the Boltzmann population excess is only ~10 spins per million, the *macroscopic* number of hydrogen nuclei within even a thin 1-mm voxel is enormous. This turns a subtle microscopic bias into a robust net magnetization that precesses coherently and induces a detectable voltage in the receive coil. In practice, this collective phenomenon—rather than the

magnitude of single-spin interactions—enables the high quality, high-contrast images that define MRI in clinical use (*e.g*., Haacke *et al*., 1999; Brown & Semelka, 2010).

Benefits and tradeoffs at higher field strengths

Signal-to-noise ratio (SNR) generally improves with field strength, which is why 3 T scanners can deliver higher spatial resolution and/or reduced scan times compared with 1.5 T in many neuro and musculoskeletal applications. However, higher field also introduces practical challenges:

- *Specific Absorption Rate* (SAR): RF power deposition increases with frequency, constraining flip angles and repetition times in some sequences.
- B_0 *and* B_1 *inhomogeneity:* Field nonuniformities can degrade image uniformity and complicate quantitative measurements.
- *Susceptibility effects*: Enhanced at higher B_0, they can be advantageous for certain contrasts (*e.g*., SWI) but may increase artifacts near air–tissue interfaces or metallic implants.
- *Relaxation shifts*: T_1 tends to lengthen with field strength, affecting contrast timing, while T_2/T_2^* can shorten in some tissues due to microscopic susceptibility and dephasing processes (Haacke *et al*., 1999; Brown & Semelka, 2010; Edelman & Warach, 1993).

  Balancing these factors is central to protocol design, particularly when optimizing SNR, contrast, and patient safety.

Encoding, *k*-space, and reconstruction considerations

The translation from precessing magnetization to spatially resolved images relies on *gradient fields* that make the Larmor frequency and phase position-dependent (slice selection, frequency/readout encoding, phase encoding). The Fourier relationship between the acquired time-domain signal and spatial frequency space (k-space) underpins image reconstruction and informs how sampling strategies, bandwidth, gradient performance, and echo times impact resolution and artifacts (Liang & Lauterbur, 2000; Bernstein, King, & Zhou, 2004; Gallagher *et al*., 2008). Practical additions such as partial Fourier, parallel imaging, and optimized gradient waveforms further trade SNR for speed or artifact reduction, depending on the clinical question.

Contrast mechanisms and clinical relevance

By manipulating TR, TE, and flip angle, MRI selectively emphasizes T_1, T_2, T_2^*, or proton density differences among tissues. This flexibility explains MRI's dominance in:

- Neurology: lesion detection, demyelination, edema, ischemia (DWI), microhemorrhage (SWI).
- Orthopedics/MSK: ligaments, cartilage, marrow pathology with multiplanar fidelity.
- Cardiovascular MRI: morphology, function, perfusion, and viability; angiography without ionizing radiation.
- Spectroscopy (MRS): noninvasive metabolic profiling.
- Interventional MRI: real-time guidance with high soft-tissue contrast (Edelman & Warach, 1993; Kijowski *et al*., 2014; Puntmann *et al*., 2020; Danielsen & Ross, 1999; Jolesz, 2011). Gadolinium-based contrast agents (GBCAs) further modulate T_1 to enhance lesion conspicuity; when used, sequence timing and safety considerations must be integrated into study design (Runge, 2018).

Limitations of the present calculations

The examples worked intentionally simplify the physics to convey intuition:

- They assume a *homogeneous* B_0 and uniform tissue properties, neglecting local susceptibility, motion, and diffusion effects.
- Coil sensitivity, loading, and parallel reception are not modeled, though they significantly affect SNR and spatial variation.
- The treatment focuses on *equilibrium* magnetization; transient phenomena (*e.g.*, preparation pulses, inversion recovery, magnetization transfer) are outside scope.
- Quantitative mapping ($T_1/T_2/T_2^*$) is not derived, and no corrections are applied for B_1 inhomogeneity or slice-profile imperfections (Haacke *et al.*, 1999; Bernstein, King, & Zhou, 2004).These simplifications are adequate for didactic clarity, but more complete analyses should incorporate relaxation dispersion with field strength, diffusion weighting, susceptibility modeling, and system hardware characteristics when precision is required.

Educational value and future directions

From a pedagogical perspective, explicitly connecting *spin physics → magnetization → RF excitation → relaxation → gradients → k-space* helps learners see how each layer contributes to the final image. Looking ahead, the field continues to evolve toward:

- *Quantitative MRI* (*e.g.*, parametric T_1/T_2 mapping) and *MR fingerprinting* to reduce dependence on qualitative contrast.
- *Advanced reconstruction* strategies (parallel imaging, constrained reconstructions) to accelerate acquisition while controlling artifacts.
- *Pulse-sequence innovation* to tailor contrast and mitigate SAR or susceptibility penalties at higher field strengths (Liang & Lauterbur, 2000; Bernstein, King, & Zhou, 2004; Haacke *et al.*, 1999). These directions strengthen the link between underlying physics and reproducible, clinically meaningful biomarkers.

Conclusion

This module has been both intellectually enriching and professionally motivating. As someone intending to pursue a career in Medical Physics—particularly within the fields of Medical Imaging or Instrumentation—the topics explored here align directly with my long-term academic and professional goals. The material provided a clear and rigorous foundation in the physical principles governing Magnetic Resonance Imaging, from the behavior of nuclear spin systems to the mechanisms through which MR signals are acquired, processed, and ultimately reconstructed into clinically meaningful images.

Beyond strengthening *a* conceptual understanding, this module deepened *in an* appreciation for the technical sophistication and interdisciplinary nature of MRI. The interplay between physics, engineering, mathematics, and physiology becomes especially evident when examining how subtle quantum-mechanical interactions scale to produce robust diagnostic information. Engaging with these principles in detail has reinforced my interest in contributing to the advancement of imaging technologies, whether through improved instrumentation, optimized acquisition strategies, or enhanced signal processing techniques.

Overall, the knowledge and perspectives gained throughout this module have solidified my commitment to continue exploring the field of Medical Physics and to pursue opportunities that support innovation in diagnostic imaging and patient care.

References

Bernstein, M. A., King, K. F., & Zhou, X. J. (2004). *Handbook of MRI pulse sequences*. Elsevier Academic Press.

Bibiloni, A., Pomi, A., & Oliver, P. M. (2003). *Foundations of quantum mechanics for medical imaging*. Springer Science & Business Media.

Brown, M. A., & Semelka, R. C. (2010). *MRI*: *Basic Principles and Applications* (4th ed.). Wiley-Blackwell.

Cherry, P. D., Sorenson, J. A., & Phelps, M. E. (2012). *Physics in nuclear medicine* (4th ed.). Elsevier Saunders.

Cobas, C. (2020). *NMR signal processing, prediction, and structure verification with machine learning techniques*. Magnetic Resonance in Chemistry, **58**(**6**): 512-519. Bloembergen, N.,

Dawson, M. J. (2013). *Paul Lauterbur and the invention of MRI*. The FASEB Journal, **27**(**5**), 1697-1700.

Edelman, R. R., & Warach, S. (1993). *Magnetic resonance imaging* (1). New England Journal of Medicine, **328**(**11**): 785–791. https://doi.org/10.1056/NEJM199303183281108

Edelman, R. R., & Warach, S. (1993). *Magnetic resonance imaging* (1). New England Journal of Medicine, **328**(**11**): 785–791. https://doi.org/10.1056/NEJM199303183281108

Edmonds, A. R. (1993). *Angular momentum in quantum mechanics*. Princeton University Press.

Gallagher, T. A., Nemeth, A. J., & Ferris, N. J. (2008). *An introduction to the Fourier transform in MRI. Radiographics*, **28**(**3**): 923–931. https://doi.org/10.1148/rg.283075131

Gudiño, A., Smith, J. T., & Rutt, B. K. (2023). *Gradient field design and optimization in MRI*. Magnetic Resonance in Medicine, **89**(**2**): 512–529.

Haacke, E. M., Brown, R. W., Thompson, M. R., & Venkatesan, R. (1999). *Magnetic resonance imaging: Physical principles and sequence design*. John Wiley & Sons.

Haacke, E. M., Brown, R. W., Thompson, M. R., & Venkatesan, R. (1999). *Magnetic Resonance Imaging: Physical Principles and Sequence Design*. Wiley-Liss.

Haacke, E. M., Brown, R. W., Thompson, M. R., & Venkatesan, R. (1999). *Magnetic resonance imaging: Physical principles and sequence design*. Wiley-Liss.

Haacke, E. M., Brown, R. W., Thompson, M. R., & Venkatesan, R. (1999). *Magnetic resonance imaging*: *Physical principles and sequence design*. Wiley-Liss.

Hashemi, R. H., Bradley, W. G., & Lisanti, C. J. (2010). *MRI*: *The Basics* (3rd ed.). Lippincott Williams & Wilkins.

Hoult, D. I., & Bhakar, B. (1997). *NMR signal reception: Virtual photons and coherent spontaneous emission.* Concepts in Magnetic Resonance, **9**(**5**), 277–297. https://doi.org/10.1002/(SICI)1099-0534(1997)9:5<277::AID-CMR1>3.0.CO;2-W.

Hughes, E., Möller, J., & Schmidt, T. (2009). *Quantum mechanics in biomedical sciences*. Oxford University Press.

Katti, G., Ara, S. A., & Shireen, A. (2011). *Magnetic resonance imaging* (MRI): *A review*. International Journal of Dental Clinics, **3**(**1**): 65–70.

Liang, Z. P., & Lauterbur, P. C. (2000). *Principles of magnetic resonance imaging*: *A signal processing perspective*. Wiley-IEEE Press.

Liang, Z. P., & Lauterbur, P. C. (2000). *Principles of magnetic resonance imaging*: *A signal processing perspective*. IEEE Press.

Nishimura, D. G. (2010). *Principles of Magnetic Resonance Imaging*. Stanford University.

Purcell, E. M., & Pound, R. V. (1948). *Relaxation effects in nuclear magnetic resonance absorption*. Physical Review, **73**(**7**): 679–712.

Rabi, I. I. (2025). *The birth of magnetic resonance*: *A historical perspective*. Columbia University Press.

Rigden, J. S. (1986). *Isidor Isaac Rabi*: *The man in the magnetic resonance*. Physics Today, **39**(**10**): 78–80. https://doi.org/10.1063/1.2815185

Rinck, P. A. (2018). *Magnetic resonance in medicine. A critical introduction*. The Basic Textbook of the European Magnetic Resonance Forum (12th ed.).

Vasanawala, S. S., Pauly, J. M., & Nishimura, D. G. (1999). *Linear combination steady-state free precession MRI*. Magnetic Resonance in Medicine, **42**(**5**): 876–883.

Weingärtner, S. (2013). *From NMR to MRI*: *The history and physics of magnetic resonance imaging*. Springer Science & Business Media.